The Interplay of Electrostatics and Chemical Positioning in the Evolution of Antibiotic Resistance in TEM β-Lactamases

Samuel H. Schneider,[a,b] Jacek Kozuch,[a,c] Steven G. Boxer*

Chemistry Department, Stanford University, Stanford, CA, 94305, USA

[a] These authors contributed equally to this work.

* corresponding author sboxer@stanford.edu

[b] Present address: Department of Pharmaceutical Chemistry, University of California San Francisco, San Francisco, CA, 94158, USA

[c] Present address: Experimental Molecular Biophysics, Department of Physics, Freie Universitat Berlin, Arnimallee 14, 14195 Berlin, Germany

Abstract:

The interplay of enzyme active site electrostatics and chemical positioning are important for understanding the origin(s) of enzyme catalysis and the design of novel catalysts. We reconstruct the evolutionary trajectory of TEM-1 β-lactamase to TEM-52 towards extended-spectrum activity to better understand the emergence of antibiotic resistance and to provide insights into the structure-function paradigm and non-covalent interactions involved in catalysis. Utilizing a detailed kinetic analysis and the vibrational Stark effect, we quantify the changes in rate and electric fields in the Michaelis and acyl-enzyme complexes for penicillin G and cefotaxime to ascertain the evolutionary role of electric fields to modulate function. These data are combined with MD simulations to interpret and quantify the substrate-dependent structural

changes during evolution. We observe that evolution utilizes a large preorganized electric field and substrate-dependent chemical positioning to facilitate catalysis. This governs the evolvability, substrate promiscuity, and protein fitness landscape in TEM β-lactamase antibiotic resistance.

Introduction:

The origins of the enormous catalytic capacity of enzymes remains a long-standing question. Unravelling these origins is essential to our ability to design and engineer proteins with diverse functions, as well as rationalize the evolutionarily-acquired mutations that lead to altered functions such as novel substrate scopes and chemistry, solvent adaptation, thermal-stability, and improved rates, as demonstrated with the many successes of directed evolution.[1-2] A physical picture of enzyme evolution requires new observables that can link evolutionary changes in catalysis to local interactions arising from mutations.

Recent experimental work, based on the electrostatic catalysis model and the vibrational Stark effect (VSE), has quantified the electrostatic contribution to catalysis in the model enzyme, ketosteroid isomerase (KSI),[3-4] and more generally for enzymes such as serine proteases and dehalogenases.[5-6] The VSE method utilizes high-frequency and local vibrational reporters, such as carbonyls (C=O), to quantify the electric field in enzyme active sites. Carbonyls are the functional moieties of many enzymatic reactions, including KSI and the β-lactamases discussed in detail in the following, making them ideal for investigating electrostatic catalysis. Measurement of the active site electric field is achieved through calibration of the carbonyl-containing molecule by VSE spectroscopy, using a well-defined external electric field, vibrational solvatochromism and MD simulations.[5, 7] This approach provides an electric field-frequency calibration curve from which the environment's electric field projected onto the probe bond can be directly quantified using vibrational (IR or Raman) spectroscopy.[6] By combining the free-

energy barrier of activation, $\Delta G^{\ddagger}$, from steady-state kinetics and transition-state (TS) theory with measurements of the active site electric field ($\vec{F}_{enz}$) for a series of wild-type (WT) and mutant enzymes, the contribution of electrostatic catalysis to accelerate a reaction ($\Delta\Delta G^{\ddagger}$) can be modeled according to,[6, 8]

$$\Delta\Delta G^{\ddagger} = -\left[\left(\vec{F}_{enz,TS} \cdot \vec{\mu}_{TS}\right) - \left(\vec{F}_{enz,RS} \cdot \vec{\mu}_{RS}\right)\right] \qquad \text{(Eq. 1)}$$

where $\vec{\mu}_{TS}$ and $\vec{\mu}_{GS}$ are the TS and reactant-state (RS) dipole moment for bonds that change charge distribution over the course of the reaction coordinate.

All previous studies using the VSE approach have been performed on wild-type and site-directed mutant enzymes,[6] where the latter were all deleterious to the overall enzymatic function and do not necessarily reflect those acquired over the course of evolution. However, the multi-dimensional evolutionary fitness landscape can modulate favorable enthalpic and entropic effects by improving the electrostatic environment and chemical positioning within the enzyme active site. Chemical positioning refers to the energetic effects on catalysis of placing reactive groups in close proximity and correct orientations relative to the bound substrate. While both electrostatic catalysis and chemical positioning are important, we start with the hypothesis that, similar to KSI,[6] if electrostatic TS-stabilization is the primary driving force for navigating the evolutionary fitness landscape, then an enzyme's evolution towards improved function (i.e. lower $\Delta G^{\ddagger}$) would correspond to a proportional increase in the active site electric field (note that negative electric fields correspond to stabilizing interactions).

The enzymes we have chosen to test this hypothesis are β-lactamases, which play a clinical role in the emergence of antibiotic resistance.[9-10] TEM-1, a class A and the first isolated and genetically-characterized β-lactamase, has served as a model enzyme for understanding protein evolution towards extended-spectrum β-lactamase (ESBL) activity, one of the mechanisms for achieving antibiotic resistance.[11-22] There are now over 240 TEM β-lactamase clinical variants (and over 7100 identified β-lactamases in total[23]) that endow extended-

spectrum activity against multiple β-lactams (including penicillins, cephalosporins, and monobactams) as well as inhibitor-resistance (e.g. clavulanic acid).[24] TEM-1 has narrow spectrum penicillinase activity, i.e. against penicillin G (PenG) and ampicillin, and its evolution towards new function against other classes of β-lactam antibiotics, such as cephalosporins, has been observed both in clinical isolates and directed evolution.[25-26]

One of the most well-studied ESBL evolutionary trajectories is from TEM-1 over the course of three mutations, E104K, G238S, and M182T, to TEM-52 (E104K/G238S/M182T Ambler notation;[27] Figure 1a), resulting in both decreased penicillinase activity and increased hydrolysis of the third-generation cephalosporin, cefotaxime (CTX). We use the functionally critical β-lactam C=O (Figure 1b)[25, 28-29] as an IR probe of the active site electric field. The general mechanism and reaction coordinate for class A β-lactamases are shown in Figure 1c. Upon binding, the β-lactam antibiotic forms the non-covalent enzyme-substrate complex (ES) which is first acylated via ring-opening of the β-lactam by the active site serine (S70), forming an acyl-enzyme intermediate (AE). The AE complex is subsequently deacylated via a nucleophilic water molecule activated by a nearby glutamate (E166), followed by product release.[10] Note that in contrast to KSI which uses amino-acid side-chains to H-bond with the substrate/inhibitor, TEM β-lactamases interact with the bound β-lactam C=O through backbone amides of S70 and A237. These backbone amides serve as hydrogen-bond donors and are maintained throughout the course of natural evolution, although slight changes in their position may accompany mutations elsewhere in the protein.

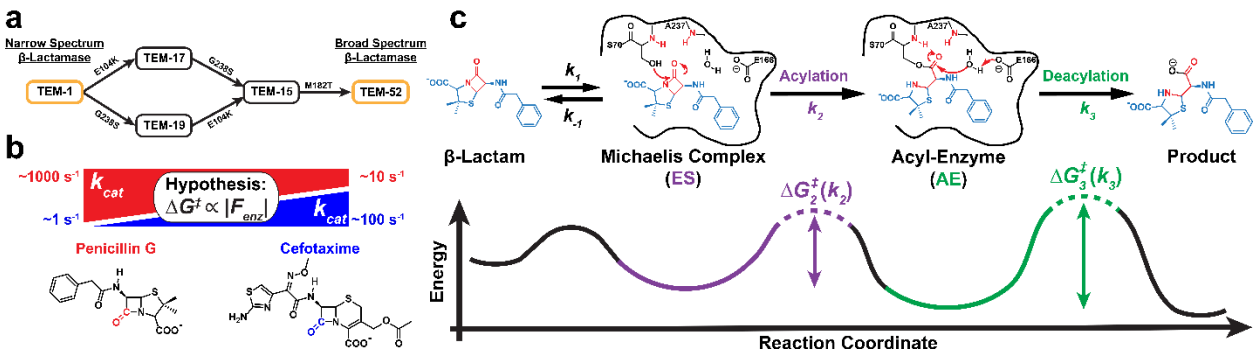

Figure 1. Evolutionary trajectory and reaction mechanism of TEM-1 to TEM-52 β-lactamase. (a) *The most-probable evolutionary trajectory from TEM-1 to TEM-52 with the acquisition of three mutations (E104K, G238S, and M182T) which alters the substrate scope of TEM β-lactamase from narrow spectrum to broad spectrum activity against β-lactam antibiotics.* ***(b)*** *Order of magnitude change in rate-constant for the hydrolysis (k_{cat}) of penicillin G (PenG; red) and cefotaxime (CTX; blue) over the course of evolution from TEM-1 to TEM-52[30] with the hypothesized change in free energy barrier of activation ($\Delta G^{\ddagger}$ from TS-theory) proportional to the active site electric field, $|F_{enz}|$. Reactive carbonyls of the β-lactams are highlighted for clarity.* ***(c)*** *Mechanism of class A β-lactamases and reaction coordinate diagram for PenG hydrolysis. The Michaelis complex (ES; non-covalent) and acyl-enzyme (AE; covalent) are illustrated in reference to functionally important active site residues formed via the amide backbone nitrogens of S70 and A237 as well as key catalytic residues, S70 and E166, necessary for the acylation and deacylation reactions, respectively. The functional β-lactam ring and oxyanion hole are shown in red and all other substrate moieties in blue, where chemical functionalization is altered across antibiotic classes (e.g. penicillins, cephalosporins, monobactams, etc.). The two chemical steps, acylation (k_2; purple) and deacylation (k_3; green) can be related to their respective activation free energy barriers through transition-state theory which proceed through tetrahedral intermediates at each step (dotted lines, see Scheme S1 for details). Barrier heights not drawn to scale.*

In the following, we use two substrates, PenG and CTX, to monitor the evolutionary changes to catalytic rates, the electric fields sensed by the reactive β-lactam, and chemical positioning throughout the active sites. In order to understand the mechanistic implications of these evolutionary changes we measured the Michaelis-Menten kinetic parameters and the corresponding acylation (k_2) and deacylation (k_3) rate constants for all mutants utilizing both PenG and CTX as substrates. Using the VSE to monitor local catalysis-relevant electric fields and molecular dynamics (MD) simulations to evaluate changes in chemical positioning, we expand upon the physical origins of antibiotic resistance and catalysis in TEM β-lactamases.

Results:

Kinetic Decomposition of β-Lactamase Activity

Given the mechanism depicted in Figure 1c for class A β-lactamases, the Michaelis-Menten parameters, k_{cat} and K_M, correspond to:

$$k_{cat} = \frac{k_2 k_3}{k_2 + k_3} \qquad \text{(Eq. 2)}$$

$$K_M = \frac{k_3(k_{-1} + k_2)}{k_1(k_2 + k_3)} \qquad \text{(Eq. 3)}$$

The acylation (k_2) and deacylation (k_3) rate constants were determined following the previously described steady-state mass spectrometry approach (Figures S1-2).[31] At steady-state conditions, the relative concentrations of the AE and ES complexes can be directly related to the corresponding rate constants according to (Figures S3-4):

$$\frac{[AE]}{[ES]} = \frac{k_2}{k_3} \qquad \text{(Eq. 4)}$$

The kinetic results are presented pictorially in Figure 2 and summarized in Table S1 (see Methods and Figure S1-2).

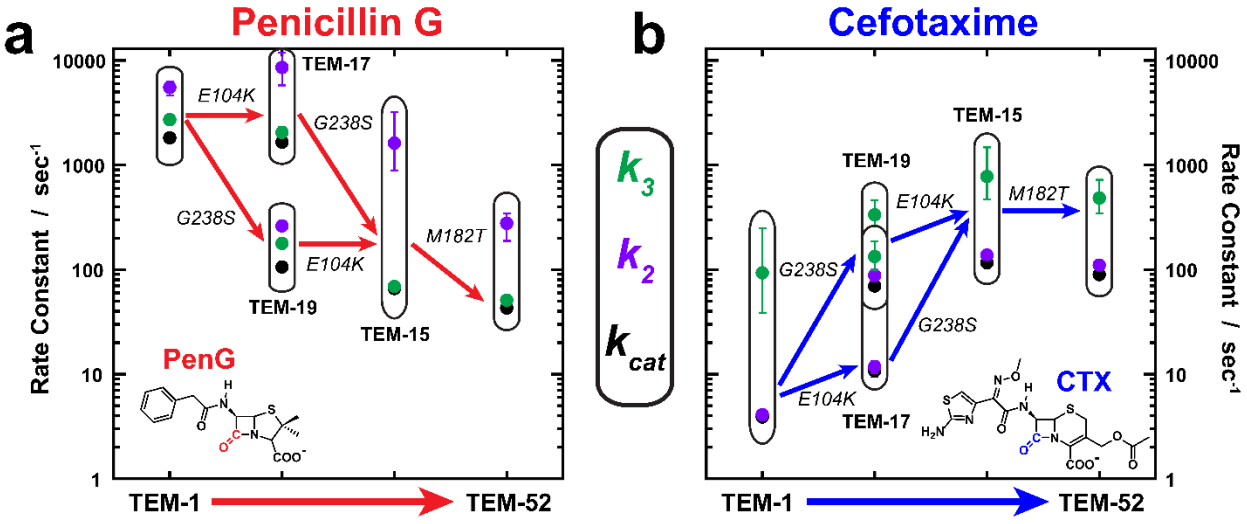

Figure 2. Evolution of the catalytic rates of β-lactam hydrolysis from TEM-1 to TEM-52. *The absolute rate constants for* ***(a)*** *PenG (red) and* ***(b)*** *CTX (blue) hydrolysis are shown for k_{cat} (black), k_2 (purple), and k_3 (green), for each TEM β-lactamase mutant along the evolutionary trajectory from TEM-1 to TEM-52 as denoted by directional arrows. Error bars represent the equivalent of 1 standard deviation (68.25% confidence interval (CI)), see the methods section,Table S1, and Figures S3-4 for details.*

As seen in Figure 2, the rate-constants all change in accordance with the observed ESBL phenotype as TEM-1 evolves towards TEM-52. In the case of PenG hydrolysis (Figure 2a), the mutations generally decrease the rate-constants in accordance with the loss of function as a narrow-spectrum penicillinase; however, the K_M decreases significantly going from TEM-1 to TEM-52, primarily as a result of the G238S mutation (Table S1). As has been previously observed with TEM-1 and PenG,[31-32] the rate-limiting step for all variants is deacylation (k_3). The extent to which acylation and deacylation change (i.e. k_2/k_3) is differentially affected by the mutations. All of the mutations, with the exception of TEM-19 (G238S), lead to k_2/k_3 perturbed away from that of TEM-1 ($k_2 \approx k_3$),[32] with the double-mutant TEM-15 being the most perturbed ($k_2/k_3 > 10$). The ratio is then partially recovered with the global suppressor mutation, M182T, which is distant from the active site but thermodynamically stabilizing,[16] leading to TEM-52 ($k_2/k_3 \approx 5$). This kinetic evaluation deconvolves some of the epistatic relationship of these mutations on function, supplementing previous studies.[12-13]

In the case of the evolutionarily improved CTX hydrolysis (Figure 2b), we observe an improvement in both binding and turnover with the two distal active site mutations, E104K and G238S, and minimal effect of M182T, relative to TEM-1. Significantly, and in contrast to that of PenG hydrolysis, the rate-limiting step for each variant is the acylation (k_2) step, such that $k_2 \approx k_{cat}$, as previously suspected by several authors.[10, 31, 33] Furthermore, the relative ratio of k_2/k_3 generally improves (i.e. towards unity) as TEM-1 evolves towards the ESBL TEM-52, primarily as a result of the G238S mutation. In terms of TEM-52's phenotype as an ESBL, i.e. increased promiscuity, the final corresponding rate-constants for both PenG and CTX converge towards the same order of magnitude, consistent with the broad-spectrum activity profile.

VSE Measurements of β-Lactamase Complexes

We utilized isotope-edited ^{12}C – ^{13}C difference spectroscopy to determine the active site electric fields using the VSE, made possible by site-specific isotope incorporation of ^{13}C into

common β-lactam antibiotics.[34] This method enables detection of a single C=O stretching frequency even amid the extensive protein backbone signal (Figure S5,7).[35] In order to trap the ES and AE species for the intrinsically slow IR measurements, we introduce the S70G and E166N mutations, respectively, to monitor the mechanistic intermediates. These kinetically incompetent background S70G or E166N mutations are denoted "TEM-# S70G" or "TEM-# E166N" relative to the evolutionary and clinically observed WT proteins TEM-1, -17, -19, -15, and -52. We infer the projected electric fields based on the observed frequency shifts using the electric-field/frequency calibration of model compounds.[36] We use the smallest and chemically simplest rigid functional moieties of the β-lactam substrate's C=O, namely the bicyclic penam/cephem core and the acylated ester for the ES and AE complexes, respectively (see ref. [36] and Figure S6).

Isotope-edited difference IR measurements of PenG and CTX in the S70G ES and E166N AE complexes with TEM β-lactamases are shown in Figure 3 (see Figure S8 for further details of spectral processing and Figure S9 for additional S70 and E166N variant spectra). Across all of the enzyme-substrate complexes we observe multiple sets of narrow (FWHM 5-16 cm^{-1}) vibrational features, with corresponding sets of ^{12}C (positive) and ^{13}C (negative) features (shown only on the bottom spectrum in each panel for clarity, Fig 3 c-f) that exhibit the expected isotope frequency shift of $\Delta\bar{\nu}$ ~ 40 cm^{-1} (Tables S1-4). These peaks are significantly narrower than the β-lactam C=O frequency in aqueous buffer (D_2O, Figure S5), which is observed at 1762 cm^{-1} with FWHM ~ 35 cm^{-1}. The multiple features are indicative of conformational heterogeneity upon binding. Previous studies with β-lactamases have indicated the possibility of multiple peaks upon substrate binding, but they could not be confidently assigned in the absence of isotopic labels.[37-38]

As shown in Figure 3 c-f, where the upper axis translates the observed frequencies into electric fields (Figure S6), we observe predominantly two distinct electric field environments for both PenG and CTX: a major population (by integrated area) in a small electric field

conformation (ca. -30 to -70 MV/cm), and minor populations at significantly larger and more stabilizing (i.e. negative sign) electric fields (ca. -140 – -175 MV/cm). The lineshapes of the lower electric field species are broad compared to the minor species experiencing much larger electric fields. The simplest interpretation of linewidth variations in proteins is that they reflect the heterogeneity of the environment around the probe.[39] For PenG, we observe minimal changes in the peak position/electric field over the course of (de)evolution for either the small or large electric field species, with the largest electric field species consistently observed at ca. -175 and -140 MV/cm (Figure 3a,b) for the ES and AE complexes, respectively. However, there is an increase in conformational heterogeneity as evidenced by additional populations with fields of ca. -160 and -30 MV/cm with introduction of G238S (i.e. TEM-19, TEM-15, and TEM-52). For PenG the negligible effect on the electric field sensed by the reactive C=O over evolution contradicts the hypothesized changes expected based on the observed rate decrease; the implications of this are discussed below. For CTX (Figure 3c,d), we observe minimal changes in the small electric field species but significantly larger electric fields detected over the course of evolution towards TEM-52, with the largest improvement in field (ΔF(TEM-52 – TEM-1) ≈ -40 MV/cm) corresponding to the ES complex (k_2 is rate-limiting). Interestingly, the largest electric fields projected onto the CTX C=O converge towards the maximum fields experienced by PenG's C=O of ca. -175 and -145 MV/cm for the ES and AE complexes, respectively; the corresponding conformational heterogeneities converge in a similar way. The magnitude of the electric field in the high-field population in TEM is consistent or even considerably larger than that of other proteins with similar oxyanion holes comprised of backbone amides (ca. -90 to -120 MV/cm).[5]

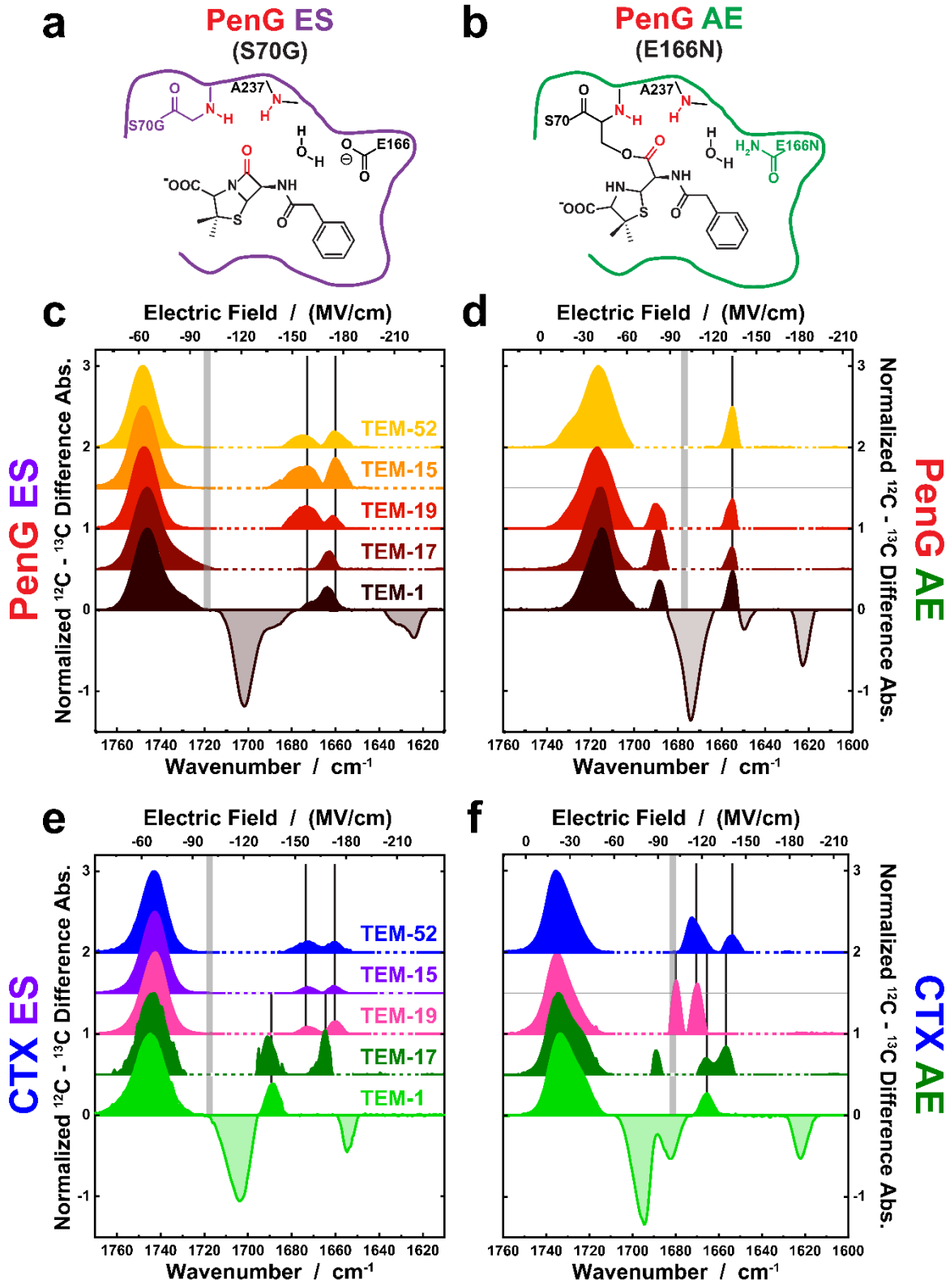

Figure 3. Isotope-edited IR difference spectroscopy of the TEM β-lactamases. (a,b) *Schematic illustration of the active site environment of TEM β-lactamases in the* ***(a)*** *ES and* ***(b)***

AE complexes with PenG and the background mutations S70G and E166N required for FTIR spectroscopy. The oxyanion hole, composed of backbone amides from S70 and A237, relative to the substrate C=O are shown in red. ***(c-f)*** *The vibrational frequencies and corresponding electric fields for* ***(c, d)*** *PenG and* ***(e, f)*** *CTX in the* ***(c, e)*** *ES (S70G) and* ***(d, f)*** *AE (E166N) complexes across evolutionary variants from TEM-1 to TEM-52. IR spectra are shown as a ^{12}C-normalized difference absorbance with an example ^{12}C – ^{13}C spectra shown for TEM-1 complexes and otherwise depicted with only the positive (^{12}C) features for clarity with dashed horizontal axes indicating negative features that have been removed for simplicity (see Figure S7 for full ^{12}C – ^{13}C difference spectra). The top axis is the electric field corresponding to the ^{12}C-isotope of the corresponding VSE calibrated probe (Figure S6). The panels are sub-divided between those C=O species corresponding to small or large electric fields (-100 MV/cm; vertical gray bars) to broadly classify the results. Vertical black lines indicate large electric field species changes between evolutionary mutations. The TEM-15 E166N mutant was not measured due to the protein's instability and likely aggregation, observed as increasing protein-specific spectral changes and loss of 280 nm absorbance over time.*

MD Simulations of β-Lactamase Complexes – Effects of S70G and E166N Mutations

We utilized MD simulations to provide a structural basis for interpreting the IR and kinetic results as well as monitoring changes in chemical positioning between the start and end points of the evolutionary trajectory (TEM-1 and -52; 1 μs MD runs of each). The MD simulations provide two primary results: (1) they compare and contrast the extent to which the necessary background mutations, S70G and E166N, bias the conformational sampling relative to their WT variants and assess the functional relevance of the species detected by IR; and (2) they help elucidate the structural origins and effect of chemical positioning on catalysis and evolution, which cannot be fully described by electrostatics as evidenced by the VSE results.

Protein-ligand complexes were simulated starting from an initial ligand pose based on crystallographic coordinates of PenG-acylated TEM-1 E166N (PDB ID: 1FQG) and CTX-acylated Toho-1 E166A (PDB ID: 1IYO), which were modelled into the corresponding variants in both the non-covalent ES and covalent AE states (see Methods). We focus on the oxyanion

hole interactions that are important for function and most directly relevant to interpreting the VSE results,[40] namely, the O – N distances between the β-lactam C=O and the backbone amide nitrogens of S70 and A237. To compare the background mutants with WT, the O – N distances were measured for the ES complexes of WT and S70G, and the AE complexes of the WT and E166N; the comparison is made for both TEM-1 and TEM-52 (Figure 4a-d). Based on these MD trajectories, 2D-correlation plots of the $O_{\beta lactam\ C=O}$ – N_{A237} ("O – N237") versus the $O_{\beta lactam\ C=O}$ – N_{S70} ("O – N70") distances were generated for each protein-ligand complex (Figure 4e-h), and the average structures for each conformation were compared between the mutants and WT protein complexes (Figure S10-12). Comparison of the commonly observed conformations, for both the S70G and E166N mutants and the respective WT proteins, enables a structure-guided approach to interpret the IR and kinetic results as discussed below. While it is tempting to directly calculate the active site electric field as experienced by the β-lactam C=O in the MD simulations, accurate calculation of electric fields when short H-bonds are involved in catalysis requires more advanced simulation forcefields and levels of theory.[41-46]

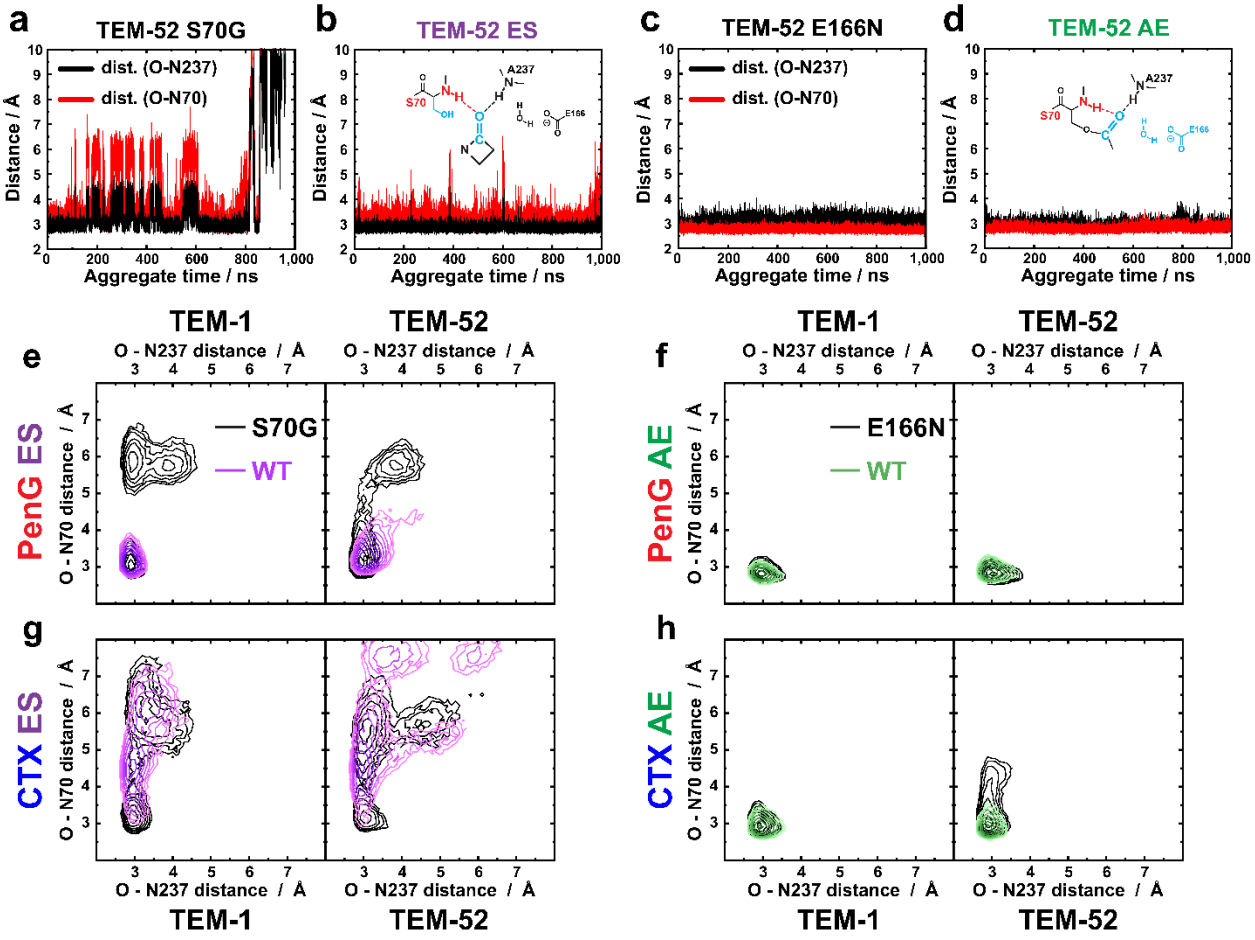

Figure 4. MD structure-guided approach to assess the effect of background and evolutionary mutations on the ES and AE complexes. (a-d) *Example MD trajectories of the TEM-52 $O_{\beta lactam\ C=O}$ – N distances between the oxyanion hole comprised of the backbone N-H of S70 (red) and A237(black), and the β-lactam C=O of PenG in the ES and AE complexes. Comparison of the background mutations* ***(a)*** *TEM-52 S70G ES and* ***(c)*** *TEM-52 E166N AE relative to the* ***(b, d)*** *TEM-52 WT ES and AE complexes, respectively, provides a means to assess perturbations to the active site environment, e.g. conformational sampling, structural fluctuations, and effects of evolutionary mutations.* ***(e-h)*** *2D correlation plots of the O – N distances as a function of background mutants (black contours) relative to the WT for the* ***(e, g)*** *ES (purple) and* ***(f, h)*** *AE (green) complexes of TEM-1 and -52 with* ***(e, f)*** *PenG and* ***(g, h)*** *CTX. Contours represent dwell times ≥400 ps on a log-scale. Average structures of overlapping conformational species were evaluated for structural similarity (see main text).*

A comparison of MD simulations of the S70G and E166N background mutants with WT complexes, which are inaccessible to our IR measurements, provides insights into states that

are due to the required background mutations versus those that are catalytically permissive (Figure 4). In these simulations, the background mutations introduce exaggerated conformational heterogeneity relative to the WT, primarily evident in the ES complexes, where the functional β-lactam C=O is displaced from the oxyanion hole due to increased water accessibility (Figure S12). This results in the C=O forming H-bonds to a water molecule located in the active site, which would be expected to result in smaller electric fields than those observed in the oxyanion hole, consistent with the VSE measurements and vibrational solvatochromism in water (Figure 3, Figure S6,12-13).[36] When we biased the WT ES complexes to start from structures resembling these long O – N states in the S70G mutant, we find that these conformations are not maintained, and generally converge towards the shortest O – N distance species (Figure S14). This suggests that the removal of the S70 sidechain can induce additional substrate binding modes within the active site oxyanion hole, as previously suggested in the TEM-1 S70G crystal structure.[47] Importantly, the species with the shortest oxyanion hole distances (< 4 Å), likely the catalytically permissive states, are commonly observed in both the background mutants and WT TEM-1 and -52 simulations for the ES and AE complexes with PenG and CTX. The average structures are similar to the crystallographic binding geometry as observed for the TEM-1 S70G and E166N complexes with PenG (Figure S11,12).[47-48] We consider only those species shared in common as the biologically relevant and catalytically permissive species.

MD Simulations of β-Lactamase Complexes – Evolutionary Changes and Structural Plasticity

Based on the MD results, we quantify the significant ($p < 0.05$ in two-tailed t-test) and substrate-dependent structural changes from TEM-1 to TEM-52 in terms of the changes in inter-atom distances and root-mean square fluctuations (RMSF) of key atoms and residues in the active site (Figure 5, Scheme S2, Table S7-12). We emphasize in Figure 5 only those residues directly involved in the extended H-bond network to nucleophilic groups, i.e. the first

coordination sphere, with other potentially important residues reported in the Table S7-12 and Figure S15,16. These structural and dynamic changes are generally involved in modulating interactions with the catalytic residues and/or water, binding of β-lactams' amide side-chains or carboxylates, or the extensive H-bond network in the active site. Alignment of the reactive substrate C=O in TEM-1 and TEM-52 for the corresponding ES and AE complexes provides a functional and structural glimpse into how the evolutionarily-acquired mutations modulate catalytic turnover of PenG and CTX (Figure 5a,b,e,f), complementary to the VSE measurements. The changes in structural heterogeneity of key active site atoms and residues, in terms of RMSFs, are graphically presented in Figure 5,c,d,g,h to identify key differences between TEM-1 and TEM-52 in a substrate-dependent and ES- and AE-dependent manner.

The introduction of the evolutionarily-acquired mutations E104K and G238S leads to substrate-dependent structural changes across the active site. These changes primarily affect H-bonding interactions in the Ω-loop[10, 49] (E166 and N170) and surrounding H-bond network, which modulates the positioning of S70, E166, and the catalytic water with respect to the reactive C=O (Figure 5). For example, the average structures from MD simulations illustrate how the G238S mutation contributes to disrupting the backbone interaction of N170 – G238 in TEM-1, which results in the Ω-loop becoming more flexible and expanding the active site to accommodate larger substrates such as CTX (Figure 5).[10] We generally observe an increase in structural heterogeneity for interactions with PenG and CTX in TEM-52 relative to TEM-1 as evident in the RMSF, which is also associated with additional active site water molecules (Figure 5b,e,f). For CTX, interactions in ES and AE are differently affected. In the ES complex we observe minimal changes in the active site RMSFs, but there is a significant shortening of the distance of the β-lactam C=O to the S70 backbone amide (ΔD1 = -0.5 Å) as well as improved positioning of the S70 side-chain hydroxyl group for the nucleophilic attack (α = 37° → 30°; Figure 5e, Scheme S3), which approaches those observed in the TEM-1 ES-complex with PenG (Figure 5a). The shortened distance of the β-lactam C=O to the backbone amide would

be predicted to lead to an increase in the electric field of the highest-field (most red-shifted) component, consistent with the VSE results (Fig. 3). In the AE complex with CTX, there is increased solvent accessibility as evident from the presence of an additional water molecule in the vicinity of E166, N170 and CTX, which exhibits improved positioning in terms of attack distance and angle relative to those found in TEM-1 (Figure 5f), again approaching those observed in the AE-complex with PenG (Figure 5b). There are additional significant structural changes, in terms of both inter-atom distances and RMSFs that are observed more globally around the active site, consistent with the aforementioned observations and, thus, likely support the positioning of reactive groups as well as modulating substrate binding into the oxyanion hole (Scheme S2, Table S7-14, Figure S15,16). This is a result of the substrate-specific geometry of the bicyclic core (i.e. penam versus cephem), including the carboxylate geometry relative to the

β-lactam C=O, and the amide side-chain, which together differentially influence, and are influenced by the evolutionary trajectory (Table S13,14, Figure S18).

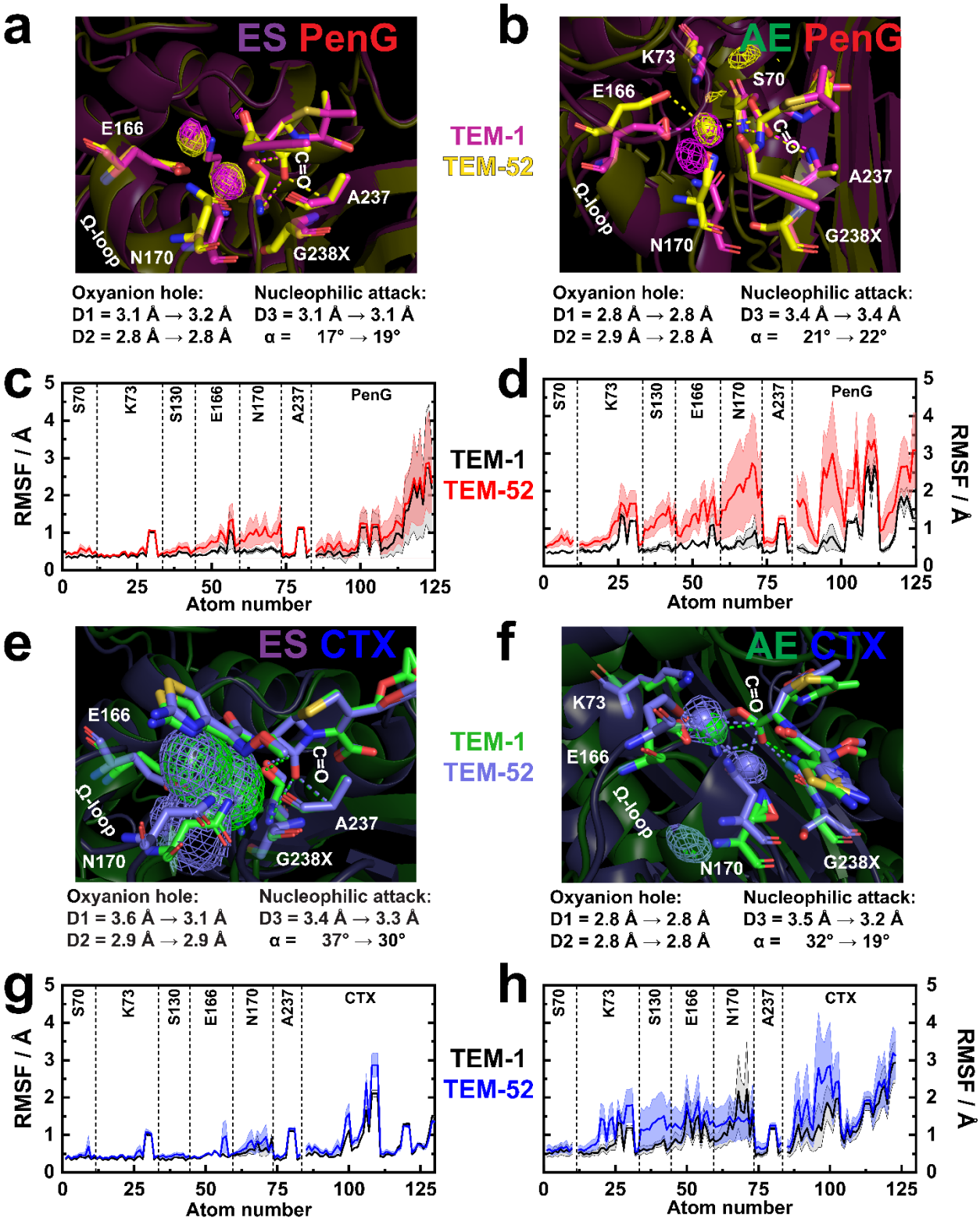

Figure 5. Catalytic interactions and active site structural heterogeneity in TEM β-lactamases as quantified via MD simulations. (a,b,e,f) *Average active site structural overlay of* ***(a,b)*** *PenG and* ***(e,f)*** *CTX in complex with TEM-1 (pink or green) and TEM-52 (yellow or purple) in the ES and AE complexes, respectively. D1 and D2 refer to the* $N_{backbone} - O_{\beta lactam\ C=O}$ *distances of the oxyanion hole between the β-lactam C=O and the S70 and A237 backbone amides, respectively. D3 and α refer to the distance and angle of the nucleophilic S70 side chain O atom or catalytic water O atom in the ES- or AE-complex, respectively, the latter relative to the substrate C=O (the plane of the β-lactam and ester C=O in the ES and AE complexes, respectively, Scheme S3). Structures are aligned according to the substrate's C=O to indicate evolutionary changes from the perspective of the reactive functional group. Averaged structures as well as extracted observables/values refer to MD aggregate times of 1 μs; except for CTX ES complexes where a total of 200 ns was used. Comparison of catalytic interactions with the oxyanion hole and nucleophilic S70 or reactive water are indicated by dotted lines and values. Solid spheres in the AE complexes represent the average water positions, and isomeshed density represents the active site regions where waters are observed in the vicinity of E166 and the substrate.* ***(c,d,g,h)*** *Absolute RMSF of active site residues and substrate atoms with respect to TEM-1 (black) and TEM-52 (red or blue) for* ***(c,d)*** *PenG and* ***(g,h)*** *CTX in the ES and AE complexes. Solid lines represent the average RMSF of a given atom across the MD trajectories with the 95% CI shown with dotted lines and shaded regions. See SI Scheme S2, Table S7-12, Figure S15,16 for further details on active site RMSF and distance changes between TEM-1 and TEM-52 with PenG and CTX.*

Discussion:

Role of Electric Fields and Structural Changes for Catalysis

Nearly all crystallographic studies of TEM β-lactamases with inhibitors and substrates exhibit only a single conformation,[47-48, 50-51] while MD simulations indicate conformational sampling and biasing as a mechanism for β-lactamase evolution.[37-38, 52-57] In order to rationalize the observed changes over the evolutionary trajectory from TEM-1 to TEM-52 we combine the kinetic, VSE, and MD results to assess the role of electrostatic, chemical positioning, and conformational effects in modulating the activation free energy barrier ($\Delta G^{\ddagger}$ from k_{cat} and TS-theory) (Figure 6, Table S2).

In the case of the evolved improvements in cefotaximase activity of TEM-52, relative to TEM-1, we observe changes in *both* the catalytically relevant active site electric field and positioning of the nucleophilic atoms, i.e. the side-chain of S70 and active site water involved in acylation (ES state) and deacylation (AE state), respectively, as summarized in Figure 6. Contrary to our expectations based on the kinetics, even in TEM-1 we observe in the IR spectra a catalytically relevant population with a high electric field projected onto the β-lactam C=O of CTX; MD simulations indicate that the catalytic inefficiency can be ascribed to mispositioned catalytic residues. Over the course of evolution, in the rate-limiting ES state, the three mutations result in non-monotonic increases in the magnitude of the largest electric fields experienced by the C=O (Figure 6a, blue arrows). This is consistent with E104K and G238S leading to an expansion of the active site to accommodate CTX,[10] allowing an improved alignment of the β-lactam C=O with the backbone amide N-H's of S70 and A237 as observed using MD and expected to generate large electric fields, consistent with what is observed by the VSE (Figure 6a, blue arrows). In addition, we observe small increases in the RMSFs of the S70 side-chain that are compensated by shortened distances and a better attack angle, i.e. improved chemical positioning, approaching those observed in the PenG complexes (Figure 6c, blue arrows). In the deacylation step, we detect improved *and* worsened electric fields over the course of evolution (Figure 6b, blue arrows), which is in line with the overall increased RMSFs of the active site (Figure 5d,h). At the same time, better positioning of the nucleophilic water, in terms of distance and attack angle with respect to the acyl ester C=O (Figure 6d, blue arrows), is achieved through increased solvent accommodation and entry of a second water molecule (Figure 5e,f).

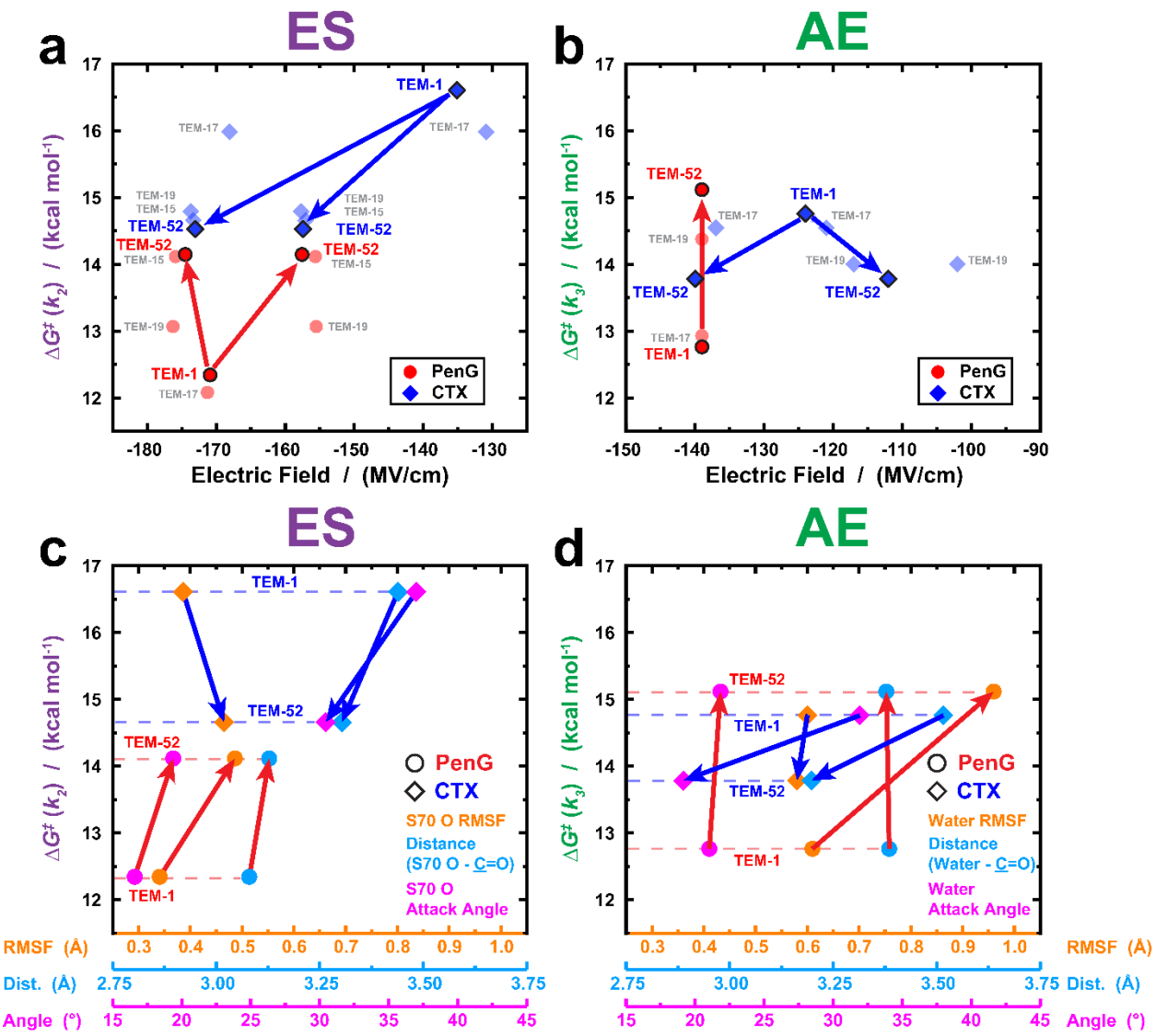

Figure 6. Substrate-dependent evolution of active site electric fields and chemical positioning in the catalysis of TEM β-lactamase. (a,b) *The non-monotonic correlation between the large catalytically relevant electric field species and free energy barriers of activation from steady-state kinetics and TS-theory for* ***(a)*** *acylation (ES) and* ***(b)*** *deacylation (AE) with respect to PenG (red) and CTX (blue).* ***(c,d)*** *Correlation between the free energy barriers of activation and absolute changes in chemical positioning (RMSF, distances to β-lactam C=O, and attack angle) for nucleophilic attack of* ***(c)*** *S70 or* ***(d)*** *active site water from MD simulations of the ES and AE complex, respectively, for hydrolysis of PenG (red circles) and CTX (blue diamonds). The RMSF (orange), distance to β-lactam C=O (light blue), and nucleophilic attack angle (pink; defined according to the plane of the C=O, Scheme S3) represent averages across the MD trajectories as discussed in Figure 4-5. Catalytic waters are*

assigned according to their proximity to E166, K73, N170, and the substrate C=O as described according to Figure 5. Arrows denote the direction of evolution from TEM-1 to TEM-52 and are colored according to the substrate.

Based on previous investigations of enzymes with the VSE that employ similar reaction mechanisms (e.g. serine proteases),[6] a reduction of the activation free energy barrier by 1 kcal/mol corresponds to more stabilizing electric fields by 10 – 20 MV/cm if modulated primarily by electrostatic TS-stabilization. The observed improvements of electric field are consistent with this relative change in activation free energy barrier for acylation (rate-limiting) and deacylation for CTX hydrolysis, so that increased RMSFs are compensated by improved distances and attack angle of nucleophilic atoms via global structural changes throughout the enzyme active site (Figure S15-17). For deacylation, the divergence of electric fields over the course of evolution may suggest that improved chemical positioning is the major contribution to improved rates.

In the case of the PenG hydrolysis, where deacylation is rate-limiting (Figure 2a), there is no obvious selective pressure to preserve the catalytic efficiency of TEM-1 during the evolutionary trajectory to TEM-52. We observe that the E104K mutation greatly alters the k_2/k_3 ratio, resulting in $k_3 \approx k_{cat}$, consistent with either a reduced electric field magnitude at the β-lactam C=O or mispositioning of E166 and the nucleophilic water molecule for deacylation. The β-lactam C=O vibration is only sensitive to the electric field projected onto its bond axis, and therefore changes occurring orthogonal to or far from the reactive C=O probe, such as changes in the positioning of E166, S70, or the catalytic water, may not be spectroscopically observed. Therefore, the apparent absence of a change in electric field for the catalytically relevant high-field population in the IR spectra (Figure 6a,b) suggests that the changes in chemical positioning of active site residues are a more likely basis for the observed rate changes. This is consistent with the changes in the RMSFs of the nucleophilic atoms (Figure 6c,d, orange, red

arrows), such as the acylating serine, in line with decreased k_2, and overall increased active site heterogeneity as observed in the MD that accompany the evolution from TEM-1 to TEM-52 (e.g. K73, E166, N170; Figure 5c,d, S15-17, Table S7-12). This is also consistent with the observation that G238S is primarily responsible for the reduction in both k_2 and k_3, which are the primary contribution to lowering K_M (Figure S19 and Table S15). Recently reported studies using time-resolved electrospray ionization with H/D exchange on TEM-1 with ampicillin and cephalexin are consistent with these structural changes and implications in the AE complex, with efficient deacylation (i.e. TEM-1 with PenG) being associated with tighter active site interactions as evident from decreased deuterium uptake.[58] This increased active site heterogeneity results in PenG becoming more inhibitor-like for TEM-52 relative to TEM-1, i.e. a high on-rate (k_1) but lower turnover ($k_{cat} \approx k_3$). The increased structural displacement and heterogeneity of the S70 and E166 side-chains and nucleophilic water are expected to break one essential aspect of the preorganized active site for acylation and deacylation, namely proper chemical positioning for catalysis.

Taken together, we see that changes in the chemical positioning of the side-chains of S70 and the catalytic water have significant kinetic consequences (Figure 6c,d) without necessarily perturbing the electric field as sensed by the β-lactam C=O (Figure 6a,b). This observation is reminiscent of the D40N mutation in KSI, which ablates the catalytic base from proton abstraction (i.e. changing the mechanism), thereby lowering the catalytic rate by 6-orders of magnitude, but has a minimal effect on the electric field projected onto the functionally important carbonyl for TS-stabilization relative to the WT enzyme.[3]

Implications for the Role of Electric Fields, the Protein Fitness Landscape, and Antibiotic Resistance

We observe that the natural evolution from TEM-1 to TEM-52 in response to new antibiotics utilizes both electrostatic effects directed at the reactive β-lactam C=O and chemical positioning

to modulate catalysis in a substrate-dependent manner. This is in contrast to prior studies of KSI, serine proteases, and 4-chlorobenzoyl-CoA dehalogenase,[6] where the observed catalytic effect could be ascribed largely to mutations that were in close contact (e.g. H-bonding) with the reactive C=O bonds. These laboratory mutations do not necessarily recapitulate the natural evolutionary trajectory of these enzymes. The observed linear free energy relationship with the active site electric field in these enzymes indicates that there is a minimal (or constant) effect of each mutation on the overall active site structural heterogeneity, so the dominant effect is through electrostatic interaction with the reactive C=O bond. In contrast, the mutations along the evolutionary trajectory from TEM-1 to TEM-52 are not directly involved in the dominant non-covalent interactions between the β-lactam C=O and backbone amides of S70 and A237 which are difficult to perturb except as a secondary consequence of changes in backbone positioning. Rather, these mutations modulate binding interactions across the active site in a substrate-dependent manner, indicative of the structural plasticity of the TEM scaffold. These can propagate to changes in the alignment of the reactive C=O with respect to the oxyanion hole electric field, as observed using the VSE with CTX (i.e. partially attributed to the 4,6-bicyclic ring), as a result of increased active site accommodation for improved binding.

Substrate promiscuity and structural plasticity enables a starting point for evolutionary improvement,[1-2, 57, 59] which in the case of TEM-1 takes three mutations to achieve the robust cefotaximase activity in the ESBL TEM-52. As demonstrated across all the TEM variants with both PenG and CTX, the maximum observed electric fields experienced by the C=O of the functional β-lactam in both the ES and AE complexes are surprisingly large throughout the enzyme's evolution. This might be expected given that the backbone amides of S70 and A237 are difficult to perturb without deformation of the active site's secondary and tertiary structure, and only a single mutation, either E104K or G238S, is necessary for the β-lactam C=O of CTX to achieve the largest electric fields observed with PenG of -140 to -175 MV/cm. If we were not starting with the evolved oxyanion hole of TEM-1 for penicillinase activity, mutations would be

required to both position the C=O of CTX into the oxyanion hole (i.e. if it could not fit or bind correctly) and to increase the overall magnitude of the electric field experienced by carbonyl group of the β-lactam ring. This hypothesis could be explored further in ancestral variants of TEM using ancestral sequence reconstruction (ASR)[60] to compare and contrast more long-term evolutionary changes in structure, function, and fields. During the evolution of CTX hydrolysis from TEM-1 to TEM-52, the large pre-existing oxyanion hole electric field simplifies the mutational search along the fitness landscape for improved catalytic rates – via improved alignment of the reactive C=O into the active site and correct positioning of the reactive water, S70, and E166 residues – thereby enabling the ESBL phenotype to be acquired over the course of three mutations and driving the emergence of antibiotic resistance. This implies that for a new β-lactam antibiotic to be effective against a given class of β-lactamases, i.e. to minimize the risk of resistance, it must bind in a manner that is able to simultaneously avoid the large active site electric field and unproductively position the catalytic side-chains. Across class A β-lactamases, the overall active site architectures, including the oxyanion hole and active site amino acids, are well conserved and therefore it is not surprising that many families of β-lactamase have been observed (and/or have the potential) to rapidly evolve activity towards hydrolysis of penicillins, cephalosporins, and monobactams.

Our findings of large electric fields in the oxyanion hole of TEM β-lactamases may help to rationalize how structural plasticity leads to substrate promiscuity.[57, 60] The evolutionary history leading to TEM-1 resulted in an enzyme scaffold and active site that is capable of exerting large stabilizing electric fields necessary for TSS of chemical reactions with similar substrate geometries and mechanisms. This may be the case for hydrolases and many other enzymes,[61] which utilize pre-existing catalytic architectures, such as oxyanion holes, to enable catalysis of a large substrate scope for further improvements via directed evolution.[62] As evident in the evolution of cefotaximase activity from TEM-1 to TEM-52, there is some basal level of binding and catalysis in the inherited protein scaffold (as required for evolution), which is

supported by the large electric fields observed even in TEM-1 with CTX. Instead of electric field optimization, subsequent mutations are focused on accommodating and chemical re-positioning of reactive side-chains and the substrate, with only small perturbations to the electric field sensed by the reactive C=O, to fully utilize these naturally evolved electric fields for catalysis. This interplay of electrostatic and chemical positioning to modulate the protein fitness landscape may be a general observation, as evident in the changes in active site heterogeneity in the directed evolution of *de novo* Kemp eliminases and ancestrally reconstructed β-lactamases.[57, 63-64] Combining the complementary approaches of MD simulations and the VSE with kinetic studies enables a more comprehensive molecular picture of the parameters modulating an enzyme's evolution towards new and/or improved function with implications in protein design, enzyme evolution, and antibiotic resistance.

Acknowledgement

We acknowledge helpful discussions with Peter Kasson at the UVA and the Vincent Coates Foundation Mass Spectrometry Laboratory at Stanford University. We thank extensive feedback from Dr. Zhe Ji, Jacob Kirsh, and Jared Weaver during the drafting process. J.K. acknowledges the Deutsche Forschungsgemeinschaft for a Research Fellowship (KO5464/1). This work is supported in part by NIH Grant GM118044 (to S.G.B.).

Methods:

Nucleotide sequence for TEM-1 β-Lactamase:

The pBAD plasmid containing TEM-1 (pBAD-TEM-1) β-lactamase was kindly given to us by Patrice Soumillion at the Université Catholique de Louvain.[65-66] Standard PCR site-directed mutagenesis was performed on the plasmid using commercial QuikChange Lightning (Agilent) kits and protocols, which was transformed into DH10B *E. coli* cells with 15 μg/mL tetracycline

HCl selection on agar plates. This was used to introduce the evolutionarily derived mutations (E104K, G238S, M182T) and kinetically incompetent variants (S70G or E166N) in addition to a cleavable His-tag in TEM-1 β-lactamase

Protein Expression and Purification:

The pBAD-TEM plasmids were transformed into One Shot TOP10 Chemically Competent *E. coli* cells (Thermo-Fisher) using selection with 15 μg/mL Tetracycline HCl on Luria Broth (Fisher) agar plates. Unless otherwise specified, all variants of TEM β-lactamase, wild-type (S70S, E166E), acylation-impaired (S70G), and deacylation-impaired (E166N), were prepared and purified identically. A single-colony of transformed cells was grown into 5 mL overnight cultures using Terrific Broth (Fisher) with 15 μg/mL Tetracycline HCl at 37C. Overnight cultures were then inoculated into 1 L of Terrific Broth (Fisher) media with 10 μg/mL Tetracycline HCl shaking at 200 rpm and 37C until they reached an OD600 ~ 0.6 at which point protein expression was induced with 2 g per L of L-(+)-Arabinose (Sigma), and grown for 4-5 hrs at 27 C. Cells were harvested by centrifugation at 6000x g's for 30 mins and resuspended in lysis buffer (50 mM potassium phosphate, 20 mM imidazole, 500 mM sodium chloride, 10% (v/v) glycerol, pH 7.4). Cells were lysed by homogenization, and the lysate centrifuged twice for 90 mins each at 15,000x g's before sterile filtering the supernatant. The crude protein was then purified using a Ni-NTA affinity resin column, washing with 50 mM potassium phosphate (pH 7.4), 50 mM imidazole, 500 mM sodium chloride and eluted using 50 mM potassium phosphate (pH 7.4), 200 mM imidazole, 500 mM sodium chloride. Further purification was performed using anion exchange chromatography on a 5 mL HiTrap-Q HP (GE Healthcare) column and eluted using a 0-40% gradient of Buffer A (25 mM Tris (pH 8.4) 25 mM sodium chloride) to Buffer B (25 mM Tris (pH 8.4) 1 M sodium chloride) over 25 column volumes. Purified protein was exchanged into a cryoprotectant-containing storage buffer (50 mM KP_i (pH 7.4), 100 mM NaCl, 10% (v/v) glycerol) for long-term storage at -80C.

UV-vis Kinetics:

All TEM kinetics with either PenG or CTX were performed using identical buffers and preparations unless otherwise mentioned. Before kinetic measurements, the concentration of the original purified TEM β-lactamase was determined using the absorbance at 280 nm (ε_{280} = 28,085 M^{-1} cm^{-1})[67] in 50 mM potassium phosphate (pH 7.0). All buffer solutions for kinetic measurements contained 50 – 200 mM potassium phosphate (pH 7.0) and bovine serum albumin (BSA; Sigma) at 0.02 – 0.05% (w/v) in order to assist with passivation of all cuvette surfaces for the low TEM concentrations used, typically between 10 – 50 nM for PenG and 10 – 500 nM for CTX hydrolysis. Prior to use, all cuvettes and rapid-mixing tubing were passivated for at least 30 mins with a 1% (w/v) BSA solution. We assume the simplest mechanism of class A β-lactamase-catalyzed hydrolysis according to (c.f. Figure 1):[10, 68]

$$E + S \underset{k_{-1}}{\overset{k_1}{\rightleftharpoons}} ES \xrightarrow{k_2} EA \xrightarrow{k_3} E + P$$

E, S, ES, AE, and P correspond to the free enzyme, substrate, non-covalent Michaelis complex, covalent acyl-enzyme complex, and product, respectively. The apparent rate constant from steady-state kinetics corresponds to the microscopic rate constants according to Eq. 1 and 2:

Hydrolysis of PenG by TEM β-lactamases was monitored on a Cary6000i UV-vis-NIR spectrometer equipped with a stopped-flow accessory (SFA-20 Rapid Mixing Accessory from TgK Scientific). Substrate loss was monitored at 232 nm ($\Delta\varepsilon_{232}$ = -940 M^{-1} cm^{-1})[49] every 0.2 secs until completion of the reaction (i.e. $\Delta A/\Delta t = 0$). A full kinetic decomposition into k_{cat} and K_M was determined using the closed-form solution to the Michaelis-Menten equation (Eq. 5), which utilizes the Lambert function (W) to solve for the time-dependent change in substrate concentration (S_t and S_0),[69-70]

$$S_t = K_M * W\left[\frac{S_0}{K_M} exp\left(\frac{S_0 - k_{cat}t}{K_M}\right)\right] \qquad \text{(Eq. 5)}$$

Kinetic parameters k_{cat} and K_M were evaluated using a MATLAB script (see SI) and measurements were repeated 7 – 9 times and for at least two solute concentrations. Kinetic parameters presented in Table 1 represent the average and standard deviation across all measurements and solute concentrations.

Hydrolysis of CTX by TEM β-lactamases was monitored on a Lambda 25 (Perkin-Elmer) UV-vis spectrometer at 262 nm, corresponding to ring-opening of the β-lactam ($\Delta\varepsilon_{262}$ = -7250 M^{-1} cm^{-1}),[49] for 16 substrate concentrations (15-1500 μM). Initial rates were determined for the first 10-30 secs of the single-wavelength kinetic trace for all substrate concentrations. Standard Michaelis-Menten plots were utilized to determine kinetic parameters for TEM-19, -15, and -52. Kinetic constants for TEM-1 and TEM-17 were determined using Lineweaver-Burke analysis because of the high K_M (ca. 1-2 mM), such that rates corresponding to saturating substrate concentrations (i.e. rate approaches k_{cat}) could not be measured. Kinetic parameters were averaged from three separate fits and errors represent the standard deviations across measurements.

Steady-state mass spectrometry:

Mass spectrometry (MS) was performed in the Stanford University Mass Spectrometry facility on a Waters Single Quadrupole LC-ESI/MS instrument. All protein LC-MS for assessing purity was performed at ~ 20 μM concentrations in water following ion-exchange chromatography and assessed using either the Intact Mass (Protein Metrics) or MassLynx (Waters) software suites.

Measurement of the proportions of non-covalent and covalent TEM-substrate complexes were performed similarly to that of Saves *et al*.[31] TEM β-lactamase was added to a solution containing an excess of substrate in 50 – 200 mM potassium phosphate buffer (pH 7.0), mixed gently, and then the reaction was quenched through addition of one volume equivalent of methanol. Concentrations were chosen to ensure that the steady-state reaction would be observed for at least 20 – 40 secs and final enzyme concentrations would be approximately 20-

50 μM in at least 50 μL for sufficient LC-MS signal-to-noise. After quenching the reaction, the solution was buffer exchanged using a 3,000 Da MWCO Amicon (Millipore) spin filter to achieve a 1:1 (v/v) mixture of water/methanol before quantification using LC-MS on a reverse-phase C8 column (2.1 x 30 mm Agilent Zorbax columns with 3.5 μm Stablebond stationary phases; ESI+, 50-2000 m/z, standard cone voltage). The HPLC mobile phases consists of water and acetonitrile with 0.1% formic acid.

The relative abundance of non-covalent (ES) and covalent (AE) complexes (+ 334 or +413 Da, respectively) was determined from analysis of the unprocessed m/z data extracted using the MassLynx software and the mass envelope intensities quantified using a MATLAB script (see Figure S3 and SI).

While quantification of the [AE]/[ES] ratios may be normally distributed, the distributions of rate constants are not necessarily since both k_2 and $k_3 > k_{cat}$, i.e. $0 \leq [AE]/[ES] \leq$ infinity. As such, we utilize the uncertainty in both k_{cat} and [AE]/[ES] ratios to bootstrap a distribution of possible k_2 and k_3 values and determine the median and appropriate confidence intervals. For comparison to normally distributed statistics we report the 68% (corresponding to 1 standard deviation in a normal distribution) and 95% confidence intervals (CI) to determine k_2 and k_3 and corresponding uncertainties. Example distributions are shown Figure S4 and the MATLAB scripts used to perform the bootstrapping is presented in the SI.

FTIR spectroscopy:

FTIR spectra were recorded on a Bruker Vertex 70 spectrometer with a liquid nitrogen-cooled mercury cadmium telluride (MCT) detector; all data processing was performed using the OPUS program (Bruker). A liquid cell was prepared using two CaF_2 optical windows (19.05 mm diameter, 3 mm thickness, Lambda Research Optics, Inc.), separated by two semicircular Teflon spacers (25 and 50 μm thickness). FTIR spectra of ^{12}C- and ^{13}C-PenG and CTX, and all TEM-substrate complexes were acquired in a D_2O buffer (50 mM KP_i, 100 mM NaCl, pD 7.0)

through averaging 256-512 scans from 4000-1000 cm^{-1} with 1 cm^{-1} resolution after 600 secs of dry air purging.[34]

All protein-substrate measurements were performed similarly with a final concentration of ca. 2.3 mM TEM and a slight excess of substrate (ca. 2.5 – 3.0 mM). In the case of the TEM S70G mutants with PenG, where slow hydrolysis can be observed on the timescale of the FTIR measurements, an excess of substrate was added (ca. 10 – 25 mM PenG). Before FTIR measurements, proteins were exchanged overnight into the D_2O buffer at 4 C and were exchanged again the following day into fresh D_2O buffer to achieve optimal H/D exchange of the protein.

In order to obtain isotope-edited difference spectra (^{12}C – ^{13}C), measurements were performed on the same day from a single batch of doubly-D_2O-exchanged protein, which ensures minimal difference between the two measurements. A brief description of the process for generating the final isotope-edited difference spectra is described below. First, the ^{13}C spectrum was scaled and subtracted from the ^{12}C spectrum to remove the protein absorption. Second, residual unbound ^{12}C- and ^{13}C-β-lactam was subtracted from the difference spectra using either PenG or CTX in D_2O buffer as a reference. Third, residual changes due to H/D back-exchange of either the bound or unbound protein complex was subtracted using either (^{12}C – ^{12}C) or (^{13}C – ^{13}C) difference spectrum in the former and a protein-only reference spectrum in D_2O buffer in the latter. Finally, based on 2^{nd}-derivative analysis and the ^{12}C – ^{13}C β-lactam C=O isotope frequency shift of ~45 cm^{-1}, sets of peaks (a positive and a negative feature) were identified and baselined conservatively. This process was repeated for multiple difference spectra and subsequent baselined spectra were averaged ($n \geq 5$) to generate those presented in Figure 2 (see Table S3-6). For further details and specific examples of the spectral processing see Figure S8.

Simulation parameterization:

The initial structures for all simulations were based on the crystal structure of the TEM1(E166N)-Penicillin G acyl-enzyme complex (PDB id: 1FQG)[48]; mutants of interest were generated via the mutation option in PyMOL 2.3.2. Then, the PenG-acylated S70 was exchanged to a serine residue and amber99-ffSBildn parameters for the resulting 6 structures (TEM-1, TEM1-S70G, TEM-1 E166N, TEM-52, TEM-52 S70G, TEM-52 E166N) containing the nucleophilic active site water were obtained using the pbd2gmx option in GROMACS 2018.[71-72] Parameters for the ligands PenG and CTX were generated using AmberTools18 (ff99SB-ildn force field and AM1-BCC) based on optimized structures from DFT simulations in Gaussian09.A (b3lyp/6-311g**(2d,2p)).[73] The PenG-acylated and CTX-acylated serine residues, needed for the simulations of the acyl-enzyme states, were parameterized analogously using acetyl and methyl amine caps on the N- and C-termini of the serine group. In order to import the parameters into the protein topology files the caps were removed to obtain the acylated PenG-serine and CTX-serine building blocks. Then, backbone partial charges were adjusted to those of the serine parameters, and finally the charges of C_β and its H atoms were minimally adjusted to ensure a correct net charge of the acylated serines. Finally, when implementing the new acylated serines into the respective protein topology file, the original structural parameters of serine (besides those containing the hydroxyl H) were maintained and all additional parameters that include the PenG or CTX moiety, but exclude the serine fragment, were added to the topology file.

MD simulations:

MD simulations were performed using GROMACS 2018,[74] and were closely related to the work of the Kasson lab.[54, 75-76] Protein structures of all variants were based on the structure of TEM-1 E166N PenG acyl-enzyme complex (PDB ID: 1FQG) as explained above. For all acyl-enzyme simulations, the starting structure for the PenG-acylated S70 was taken as is from the PDB file. PenG's starting structure in the ES complex was adapted to the same conformation:

starting from the DFT optimized geometry, PenG's core was positioned such that the β-lactam C=O was located in the oxyanion hole, similar to the acyl-enzyme, and torsion angles of side-chains were changed to resemble those in the PenG-acylated case. The CTX-acylated S70 geometry was taken from the acyl-enzyme structure of Toho-1 E166A (PDB ID: 1IYO).[77] CTX's ES geometry was adapted from 1IYO using the same approach as for PenG. In this way, in all structures the β-lactam C=O was located at H-bond length of ca. 3 Å to both nitrogens of A237 and S/G70. Each protein was positioned in the center of a box with a dodecahedral unit cell of a size corresponding to a cube with walls located at distance of at least 2 nm from the protein surface. The box was filled with ca. 20500 water molecules (tip3p) and an ion strength of 0.175 M (similar to experiments) was generated using sodium and chloride ions, such that the system is net charge neutral. Each system was energy minimized using the steepest descent algorithm until all forces were below 1000 kJ mol^{-1} nm^{-1}, and then equilibrated (NVT and NPT steps, 100 ps each with protein and ligand heavy atoms restrained; second NPT over 100 ps with Cα atoms and ligand heavy atoms restrained). Here, the velocity-rescaling theromostat and Berendsen barostat were used (300K and 1 bar) with short range interactions truncated to 1.2 nm, long range electrostatics treated with Particle Mesh Ewald, and hydrogen bonds constrained used LINCS. MD production runs (using the Parrinello-Rahman barostat) were carried out over a total of 1 μs for each of the 16 structures. If the substrate left the active site (in simulations of ES states), the simulation was aborted and continued from a structure with bound ligand. In order to test (a) the stability of each of the observed conformations of the substrate (assessed via the 2D correlation plots of the oxyanion H-bond distances; Fig 4) and (b) the possibility to access additional conformations due to possible sampling of a local minimum, for example starting WT TEM-1 in a conformation only observed in TEM-1 S70G, representative structures were extracted, and ligand conformations were implanted into proteins for additional MD simulations. Each structure was then newly minimized and equilibrated, and then underwent five 50 ns MD simulations. Average structures, rms fluctuations, distances, etc. were extracted

using the tools present in the GROMACS package and additional add-ons (e.g. GROmaps[78]). 2D correlation plots were generated in OriginLabs2018.

The quantification of changes in structural displacement, either in terms of the root mean square fluctuations (RMSF) or distances between atoms, were quantified from representative trajectories and average structures (n = 3-5, each 50-200 ns), respectively, from the WT MD simulations of TEM-1 and TEM-52 with PenG and CTX in the ES and AE states (see Scheme S2 and Tables S5-8 for further details). Across each comparison, either RMSF or distance, values that were statistically significant ($p < 0.05$) were determined from a two-tailed student's t-test (see t-values for given degrees of freedom (df). Significant values were then utilized in the corresponding averages for each set of regions or interactions in the active site: K73/N132/E166/N170, oxyanion hole, β-lactam carboxylate, or β-lactam (Figure 5, 6, S12). This approach highlights the complexity of evaluating structural perturbations arising from both mutational changes over evolution and those that are substrate specific.

8. References

1. Bloom, J. D.; Arnold, F. H., In the Light of Directed Evolution: Pathways of Adaptive Protein Evolution. *Proc. Natl. Acad. Sci. U. S. A.* **2009,** *106 Suppl 1*, 9995-10000.
2. Romero, P. A.; Arnold, F. H., Exploring Protein Fitness Landscapes by Directed Evolution. *Nat. Rev. Mol. Cell. Biol.* **2009,** *10* (12), 866-876.
3. Fried, S. D.; Bagchi, S.; Boxer, S. G., Extreme Electric Field Power Catalysis in the Active Site of Ketosteroid Isomerase. *Science* **2014,** *346*, 1510-1514.
4. Wu, Y.; Boxer, S. G., A Critical Test of the Electrostatic Contribution to Catalysis with Noncanonical Amino Acids in Ketosteroid Isomerase. *J. Am. Chem. Soc.* **2016,** *138* (36), 11890-11895.
5. Schneider, S. H.; Boxer, S. G., Vibrational Stark Effects of Carbonyl Probes Applied to Reinterpret IR and Raman Data for Enzyme Inhibitors in Terms of Electric Fields at the Active Site. *J. Phys. Chem. B* **2016,** *120*, 9672-9684.
6. Fried, S. D.; Boxer, S. G., Electric Fields and Enzyme Catalysis. *Annu. Rev. Biochem.* **2017,** *86*, 387-415.
7. Fried, S. D.; Boxer, S. G., Measuring Electric Fields and Noncovalent Interactions Using the Vibrational Stark Effect. *Acc. Chem. Res.* **2015,** *48*, 998-1006.
8. Wu, Y.; Fried, S. D.; Boxer, S. G., A Preorganized Electric Field Leads to Minimal Geometrical Reorientation in the Catalytic Reaction of Ketosteroid Isomerase. *J. Am. Chem. Soc.* **2020,** *142* (22), 9993-9998.
9. Bush, K., The Importance of β-Lactamases to the Development of New β-Lactams. In *Antimicrobial Drug Resistance. Mechanisms of Drug Resistance*, Mayers, D. L., Ed. Humana Press: Totowa, NJ, 2009; Vol. 1, pp 135-144.

10. Palzkill, T., Structural and Mechanistic Basis for Extended-Spectrum Drug-Resistance Mutations in Altering the Specificity of TEM, CTX-M, and KPC β-lactamases. *Front. Mol. Biosci.* **2018,** *5*, 16.
11. Orencia, M. C.; Yoon, J. S.; Ness, J. E.; Stemmer, W. P. C.; Stevens, R. C., Predicting the Emergence of Antibiotic Resistance by Directed Evolution and Structural Analysis. *Nat. Struct. Biol.* **2001,** *8*, 238-242.
12. Dellus-Gur, E.; Elias, M.; Caselli, E.; Prati, F.; Salverda, M. L.; de Visser, J. A.; Fraser, J. S.; Tawfik, D. S., Negative Epistasis and Evolvability in TEM-1 β-Lactamase - The Thin Line between an Enzyme's Conformational Freedom and Disorder. *J. Mol. Biol.* **2015,** *427* (14), 2396-2409.
13. Steinberg, B.; Ostermeier, M., Shifting Fitness and Epistatic Landscapes Reflect Trade-offs along an Evolutionary Pathway. *J. Mol. Biol.* **2016,** *428* (13), 2730-2743.
14. Stiffler, M. A.; Hekstra, D. R.; Ranganathan, R., Evolvability as a Function of Purifying Selection in TEM-1 β-Lactamase. *Cell* **2015,** *160* (5), 882-892.
15. Bershtein, S.; Goldin, K.; Tawfik, D. S., Intense Neutral Drifts Yield Robust and Evolvable Consensus Proteins. *J. Mol. Biol.* **2008,** *379* (5), 1029-1044.
16. Brown, N. G.; Pennington, J. M.; Huang, W.; Ayvaz, T.; Palzkill, T., Multiple Global Suppressors of Protein Stability Defects Facilitate the Evolution of Extended-Spectrum TEM β-Lactamases. *J. Mol. Biol.* **2010,** *404* (5), 832-846.
17. Zimmerman, M. I.; Hart, K. M.; Sibbald, C. A.; Frederick, T. E.; Jimah, J. R.; Knoverek, C. R.; Tolia, N. H.; Bowman, G. R., Prediction of New Stabilizing Mutations Based on Mechanistic Insights from Markov State Models. *ACS Cent. Sci.* **2017,** *3* (12), 1311-1321.
18. Bowman, G. R.; Bolinc, E. R.; Hart, K. M.; Maguire, B. C.; Marqusee, S., Discovery of Multiple Hidden Allosteric Sites by Combining Markov State Models and Experiments. *Proc. Natl. Acad. Sci. U.S.A.* **2015,** *112*, 2734-2739.
19. Bowman, G. R.; Geissler, P. L., Equilibrium Fluctuations of a Single Folded Protein Reveal a Multitude of Potential Cryptic Allosteric Sites. *Proc. Natl. Acad. Sci. U.S.A.* **2012,** *109* (29), 11681-11686.
20. Hart, K. M.; Ho, C. M.; Dutta, S.; Gross, M. L.; Bowman, G. R., Modelling Proteins' Hidden Conformations to Predict Antibiotic Resistance. *Nat. Commun.* **2016,** *7*, 12965.
21. Campitelli, P.; Modi, T.; Kumar, S.; Ozkan, S. B., The Role of Conformational Dynamics and Allostery in Modulating Protein Evolution. *Annu. Rev. Biophys.* **2020,** *49*, 269-290.
22. Yang, J.; Naik, N.; Patel, J. S.; Wylie, C. S.; Gu, W.; Huang, J.; Ytreberg, F. M.; Naik, M. T.; Weinreich, D. M.; Rubenstein, B. M., Predicting the Viability of Beta-Lactamase: How Folding and Binding Free Energies Correlate with Beta-Lactamase Fitness. *PLoS One* **2020,** *15* (5), e0233509.
23. Naas, T.; Oueslati, S.; Bonnin, R. A.; Dabos, M. L.; Zavala, A.; Dortet, L.; Retailleau, P.; Iorga, B. I., Beta-Lactamase Database (BLDB) - Structure and Function. *J. Enzyme Inhib. Med. Chem.* **2017,** *32* (1), 917-919.
24. Bush, K., The ABCD's of β-Lactamase Nomenclature. *J. Infect. Chemother.* **2013,** *19* (4), 549-559.
25. Weinreich, D. M.; Delaney, N. F.; DePristo, M. A.; Hartl, D. L., Darwinian Evolution Can Follow Only Very Few Mutational Paths to Fitter Proteins. *Science* **2006,** *312*, 111-114.
26. Gniadkowski, M., Evolution of Extended-Spectrum β-Lactamases by Mutation. *Clin. Microbiol. Infect.* **2008,** *14*, 11-32.
27. Ambler, R. P., In *Beta-Lactamases*, Hamilton-Miller, J. M. T.; Smith, J. T., Eds. Academic Press: London, 1979.
28. Guthrie, V. B.; Allen, J.; Camps, M.; Karchin, R., Network Models of TEM β-Lactamase Mutations Coevolving Under Antibiotic Selection Show Modular Structure and Anticipate Evolutionary Trajectories. *PLoS Comput. Biol.* **2011,** *7* (9), e1002184.

29. Salverda, M. L.; De Visser, J. A.; Barlow, M., Natural Evolution of TEM-1 β-Lactamase: Experimental Reconstruction and Clinical Relevance. *FEMS Microbiol. Rev.* **2010,** *34* (6), 1015-1036.
30. Wang, X.; Minasov, G.; Shoichet, B. K., Evolution of an Antibiotic Resistance Enzyme Constrained by Stability and Activity Trade-offs. *J. Mol. Biol.* **2002,** *320* (1), 85-95.
31. Saves, I.; Burlet-Schiltz, O.; Maveyraud, L.; Samama, J.-P.; Promé, J.-C.; Masson, J.-M., Mass Spectral Kinetic Study of Acylation and Deacylation during the Hydrolysis of Penicillins and Cefotaxime by β-Lactamase TEM-1 and G238S Mutant. *Biochemistry* **1995,** *34*, 11660-11667.
32. Christensen, H.; Martin, M. T.; Waley, S. G., β-Lactamases as Fully Efficient Enzymes. Determination of all the Rate Constants in the Acyl-Enzyme Mechanism. *Biochem. J.* **1990,** *266*, 853-861.
33. Singh, M. K.; Dominy, B. N., The Evolution of Cefotaximase Activity in the TEM β-Lactamase. *J. Mol. Biol.* **2012,** *415* (1), 205-220.
34. Kozuch, J.; Schneider, S. H.; Boxer, S. G., Biosynthetic Incorporation of Site-Specific Isotopes in β-Lactam Antibiotics Enables Biophysical Studies. *ACS Chem. Biol.* **2020,** *15* (5), 1148-1153.
35. Buchner, G. S.; Kubelka, J., Isotope-Edited Infrared Spectroscopy. In *Intrinsically Disored Protein Analysis. Methods in Molecular Biology (Methods and Protocols)*, Uversky, V.; Dunker, A., Eds. Humana Press: Totowa, NJ, 2012; Vol. 895, pp 347-358.
36. Kozuch, J.; Schneider, S. H.; Zheng, C.; Ji, Z.; Bradshaw, R. T.; Boxer, S. G., Testing the Limitations of MD-based Local Electric Fields Using the Vibrational Stark Effect in Solution: Penicillin G as a Test Case. *J. Phys. Chem. B* **2021,** *125* (17), 4415-4427.
37. Wilkinson, A.-S.; Bryant, P. K.; Meroueh, S. O.; Page, M. G. P.; Mobashery, S.; Wharton, C. W., A Dynamic Structure for the Acyl-Enzyme Species of the Antibiotic Aztreonam with the *Citrobacter freundii* β-Lactamase Revealed by Infrared Spectroscopy and Molecular Dynamics Simulations. *Biochemistry* **2003,** *42*, 1950-1957.
38. Wilkinson, A.-S.; Simon, W.; Kania, M.; Page, M. G. P.; Wharton, C. W., Multiple Conformations of the Acylenzyme Formed in the Hydrolysis of Methicillin by *Citrobacter freundii* β-Lactamase: A Time-Resolved FTIR Spectroscopic Study. *Biochemistry* **1999,** *38*, 3851-3856.
39. Schneider, S. H.; Kratochvil, H. T.; Zanni, M. T.; Boxer, S. G., Solvent-Independent Anharmonicity for Carbonyl Oscillators. *J. Phys. Chem. B* **2017,** *121*, 2331-2338.
40. Knox, J. R., Extended-Spectrum and Inhibitor-Resistant TEM-Type β-Lactamases: Mutations, Specificity, and Three-Dimensional Structure. *Antimicrob. Agents Chemother.* **1995,** *39*, 2593-2601.
41. Richard, A. M.; Gascón, J. A., Protein Polarization Effects in the Thermodynamic Computation of Vibrational Stark Shifts. *Theor. Chem. Acc.* **2020,** *139* (1), 9.
42. Wang, X.; He, X., An Ab Initio QM/MM Study of the Electrostatic Contribution to Catalysis in the Active Site of Ketosteroid Isomerase. *Molecules* **2018,** *23* (10), 2410.
43. Wang, L.; Fried, S. D.; Markland, T. E., Proton Network Flexibility Enables Robustness and Large Electric Fields in the Ketosteroid Isomerase Active Site. *J. Phys. Chem. B* **2017,** *121* (42), 9807-9815.
44. Welborn, V. V.; Head-Gordon, T., Fluctuations of Electric Fields in the Active Site of the Enzyme Ketosteroid Isomerase. *J. Am. Chem. Soc.* **2019,** *141* (32), 12487-12492.
45. Zoi, I.; Antoniou, D.; Schwartz, S. D., Electric Fields and Fast Protein Dynamics in Enzymes. *J. Phys. Chem. Lett.* **2017,** *8* (24), 6165-6170.
46. Bhowmick, A.; Sharma, S. C.; Head-Gordon, T., The Importance of the Scaffold for de Novo Enzymes: A Case Study with Kemp Eliminase. *J. Am. Chem. Soc.* **2017,** *139* (16), 5793-5800.

47. Stec, B.; Holtz, K. M.; Wojciechowski, C. L.; Kantrowitz, E. R., Structure of the Wild-Type TEM-1 β-Lactamase at 1.55 Å and the Mutant Enzyme Ser70Ala at 2.1 Å Suggest the Mode of Noncovalent Catalysis for the Mutant Enzyme. *Acta Crystallogr. D Biol. Crystallogr.* **2005,** *61*, 1072-1079.
48. Strynadka, N. C. J.; Adachi, H.; Jensen, S. E.; Johns, K.; Sielecki, A.; Betzel, C.; Sutoh, K.; James, M. N. G., Molecular Structure of the Acyl-Enzyme Intermediate in β-Lactam Hydrolysis at 1.7 Å Resolution. *Nature* **1992,** *359*, 700-705.
49. Banerjee, S.; Pierper, U.; Kapadia, G.; Pannell, L. K.; Herzberg, O., Role of the Ω-Loop in the Activity, Substrate Specificity, and Structure of Class A β-Lactamase. *Biochemistry* **1998,** *37*, 3286-3296.
50. Page, M. G., Extended-Spectrum β-Lactamases: Structure and Kinetic Mechanism. *Clin. Microbiol. Infect.* **2008,** *14 Suppl 1*, 63-74.
51. Minasov, G.; Wang, X.; Shoichet, B. K., An Ultrahigh Resolution Structure of TEM-1 β-Lactamase Suggests a Role for Glu166 as the General Base in Acylation. *J. Am. Chem. Soc.* **2002,** *124*, 5333-5340.
52. Olmos, J. L., Jr.; Pandey, S.; Martin-Garcia, J. M.; Calvey, G.; Katz, A.; Knoska, J.; Kupitz, C.; Hunter, M. S.; Liang, M.; Oberthuer, D.; Yefanov, O.; Wiedorn, M.; Heyman, M.; Holl, M.; Pande, K.; Barty, A.; Miller, M. D.; Stern, S.; Roy-Chowdhury, S.; Coe, J.; Nagaratnam, N.; Zook, J.; Verburgt, J.; Norwood, T.; Poudyal, I.; Xu, D.; Koglin, J.; Seaberg, M. H.; Zhao, Y.; Bajt, S.; Grant, T.; Mariani, V.; Nelson, G.; Subramanian, G.; Bae, E.; Fromme, R.; Fung, R.; Schwander, P.; Frank, M.; White, T. A.; Weierstall, U.; Zatsepin, N.; Spence, J.; Fromme, P.; Chapman, H. N.; Pollack, L.; Tremblay, L.; Ourmazd, A.; Phillips, G. N., Jr.; Schmidt, M., Enzyme Intermediates Captured "On The Fly" by Mix-and-Inject Serial Crystallography. *BMC Biol.* **2018,** *16* (1), 59.
53. Chittock, R. S.; Ward, S.; Wilkinson, A.-S.; Caspers, P.; Mensch, B.; Page, M. G. P.; Wharton, C. W., Hydrogen Bonding and Protein Perturbation in β-Lactam Acyl-Enzymes of *Streptococcus pneumoniae* Penicillin-Binding Protein PBP2x. *Biochem. J.* **1999,** *338*, 153-159.
54. Cortina, G. A.; Hays, J. M.; Kasson, P. M., Conformational Intermediate That Controls KPC-2 Catalysis and Beta-Lactam Drug Resistance. *ACS Catal.* **2018,** *8* (4), 2741-2747.
55. Wang, F.; Zhou, H.; Wang, X.; Tao, P., Dynamical Behavior of β-Lactamases and Penicillin-Binding Proteins in Different Functional States and Its Potential Role in Evolution. *Entropy* **2019,** *21* (11), 1130.
56. Crean, R. M.; Gardner, J. M.; Kamerlin, S. C. L., Harnessing Conformational Plasticity to Generate Designer Enzymes. *J. Am. Chem. Soc.* **2020**.
57. Modi, T.; Risso, V. A.; Martinez-Rodriguez, S.; Gavira, J. A.; Mebrat, M. D.; Van Horn, W. D.; Sanchez-Ruiz, J. M.; Banu Ozkan, S., Hinge-Shift Mechanism as a Protein Design Principle for the Evolution of β-Lactamases from Substrate Promiscuity to Specificity. *Nat. Commun.* **2021,** *12* (1), 1852.
58. Knox, R.; Lento, C.; Wilson, D. J., Mapping Conformational Dynamics to Individual Steps in the TEM-1 β-Lactamase Catalytic Mechanism. *J. Mol. Biol.* **2018,** *430* (18 Pt B), 3311-3322.
59. Leveson-Gower, R. B.; Mayer, C.; Roelfes, G., The Importance of Catalytic Promiscuity for Enzyme Design and Evolution. *Nat. Rev. Chem.* **2019,** *3* (12), 687-705.
60. Risso, V. A.; Gavira, J. A.; Mejia-Carmona, D. F.; Gaucher, E. A.; Sanchez-Ruiz, J. M., Hyperstability and Substrate Promiscuity in Laboratory Resurrections of Precambrian β-Lactamases. *J. Am. Chem. Soc.* **2013,** *135* (8), 2899-2902.
61. Khersonsky, O.; Tawfik, D. S., Enzyme Promiscuity: A Mechanistic and Evolutionary Perspective. *Annu. Rev. Biochem.* **2010,** *79*, 471-505.
62. Chen, K.; Arnold, F. H., Engineering New Catalytic Activities in Enzymes. *Nat. Catal.* **2020**.

63. Broom, A.; Rakotoharisoa, R. V.; Thompson, M. C.; Zarifi, N.; Nguyen, E.; Mukhametzhanov, N.; Liu, L.; Fraser, J. S.; Chica, R. A., Ensemble-Based Enzyme Design can Recapitulate the Effects of Laboratory Directed Evolution *In Silico*. *Nat. Commun.* **2020,** *11* (1), 4808.
64. Otten, R.; Pádua, R. A. P.; Bunzel, H. A.; Nguyen, V.; Pitsawong, W.; Patterson, M.; Sui, S.; Perry, S. L.; Cohen, A. E.; Hilvert, D.; Kern, D., How Directed Evolution Reshapes the Energy Landscape in an Enzyme to Boost Catalysis. *Science* **2020**, *370*, 1442-1446.
65. Deschuyteneer, G.; Garcia, S.; Michiels, B.; Baudoux, B.; Degand, H.; Morsomme, P.; Soumillion, P., Intein-Mediated Cyclization of Randomized Peptides in the Periplasm of *Escherichia coli* and Their Extracellular Secretion. *ACS Chem. Biol.* **2010,** *5* (7), 691-700.
66. Mathonet, P.; Deherve, J.; Soumillion, P.; Fastrez, J., Active TEM-1 β-Lactamase Mutants with Random Peptides Inserted in Three Contiguous Surface Loops. *Protein Sci.* **2006,** *15* (10), 2323-2334.
67. Gasteiger, E.; Hoogland, C.; Gattiker, A.; Duvaud, S.; Wilkins, M. R.; Appel, R. D.; Bairoch, A., Protein Identification and Analysis Tools on the ExPASy Server. In *The Proteomics Protocols Handbook*, Walker, J. M., Ed. Humana Press: Totowa, NJ, 2005; pp 571-607.
68. Fisher, J.; Belasco, J. G.; Khosla, S.; Knowles, J. R., B-Lactamase Proceeds via an Acyl-Enzyme Intermediate. Interaction of the *Escherichia coli* RTEM Enzyme with Cefoxitin. *Biochemistry* **1980,** *19*, 2895-2901.
69. Schnell, S.; Mendoza, C., Closed Form Solution for Time-Dependent Enzyme Kinetics. *J. Theor. Biol.* **1997,** *187*, 207-212.
70. Goličnik, M., On the Lambert W Function and its Utility in Biochemical Kinetics. *Biochem. Eng.* **2012,** *63*, 116-123.
71. Abraham, M. J.; Murtola, T.; Schulz, R.; Páll, S.; Smith, J. C.; Hess, B.; Lindahl, E., GROMACS: High Performance Molecular Simulations through Multi-Level Parallelism from Laptops to Supercomputers. *SoftwareX* **2015,** *1-2*, 19-25.
72. Páll, S.; Abraham, M. J.; Kutzner, C.; Hess, B.; Lindahl, E., Tackling Exascale Software Challenges in Molecular Dynamics Simulations with GROMACS. In *Solving Software Challenges for Exascale*, Markidis, S.; Laure, E., Eds. Springer International Publishing: Switzerland 2015; Vol. 8759, pp 3-27.
73. Frisch, M. J.; Trucks, G. W.; Schlegel, H. B.; Scuseria, G. E.; Robb, M. A.; Cheeseman, J. R.; Scalmani, G.; Barone, V.; Petersson, G. A.; Nakatsuji, H.; Li, X.; Caricato, M.; Marenich, A. V.; Bloino, J.; Janesko, B. G.; Gomperts, R.; Mennucci, B.; Hratchian, H. P.; Ortiz, J. V.; Izmaylov, A. F.; Sonnenberg, J. L.; Williams-Young, D.; Ding, F.; Lipparini, F.; Egidi, F.; Goings, J.; Peng, B.; Petrone, A.; Henderson, T.; Ranasinghe, D.; Zakrzewski, V. G.; Gao, J.; Rega, N.; Zheng, G.; Liang, W.; Hada, M.; Ehara, M.; Toyota, K.; Fukuda, R.; Hasegawa, J.; Ishida, M.; Nakajima, T.; Honda, Y.; Kitao, O.; Nakai, H.; Vreven, T.; Throssell, K.; Montgomery, J. A., Jr.; Peralta, J. E.; Ogliaro, F.; Bearpark, M. J.; Heyd, J. J.; Brothers, E. N.; Kudin, K. N.; Staroverov, V. N.; Keith, T. A.; Kobayashi, R.; Normand, J.; Raghavachari, K.; Rendell, A. P.; Burant, J. C.; Iyengar, S. S.; Tomasi, J.; Cossi, M.; Millam, J. M.; Klene, M.; Adamo, C.; Cammi, R.; Ochterski, J. W.; Martin, R. L.; Morokuma, K.; Farkas, O.; Foresman, J. B.; Fox, D. J., Gaussian 09, Rev E.01. Gaussian 09, Rev E.01, Gaussian, Inc.: Wallingford, CT, 2016.
74. Lemkul, J., From Proteins to Perturbed Hamiltonians: A Suite of Tutorials for the GROMACS-2018 Molecular Simulation Package [Article v1.0]. *Living J. Comp. Mol. Sci* **2019,** *1* (1), 5068.
75. Cortina, G. A.; Kasson, P. M., Predicting Allostery and Microbial Drug Resistance with Molecular Simulations. *Curr. Opin. Struct. Biol.* **2018,** *52*, 80-86.

76. Latallo, M. J.; Cortina, G. A.; Faham, S.; Nakamoto, R. K.; Kasson, P. M., Predicting Allosteric Mutants that Increase Activity of a Major Antibiotic Resistance Enzyme. *Chem. Sci.* **2017,** *8* (9), 6484-6492.
77. Shimamura, T.; Ibuka, A.; Fushinobu, S.; Wakagi, T.; Ishiguro, M.; Ishii, Y.; Matsuzawa, H., Acyl-Intermediate Structures of the Extended-Spectrum Class A β-lactamase, Toho-1, in Complex with Cefotaxime, Cephalothin, and Benzylpenicillin. *J. Biol. Chem.* **2002,** *277* (48), 46601-46608.
78. Briones, R.; Blau, C.; Kutzner, C.; de Groot, B. L.; Aponte-Santamaria, C., GROmaps: A GROMACS-Based Toolset to Analyze Density Maps Derived from Molecular Dynamics Simulations. *Biophys. J.* **2019,** *116* (1), 4-11.